Quantifying Mechanical Properties in a Murine Fracture Healing System Using Inverse Modeling: Preliminary Work

Michael I. Miga[a,b,c,*], Jared A. Weis[a,d], Froilan Granero-Molto[d], Anna Spagnoli[d,e]
[a]Vanderbilt University, Department of Biomedical Engineering, Nashville, TN, USA,
[b]Vanderbilt University Medical Center, Department of Radiology and Radiological Sciences,
[c]Vanderbilt University Institute for Imaging Science, Nashville, TN, USA,
[d]University of North Carolina at Chapel Hill, Department of Pediatrics,
[e]Department of Biomedical Engineering, Chapel Hill, NC, USA

ABSTRACT

Understanding bone remodeling and mechanical property characteristics is important for assessing treatments to accelerate healing or in developing diagnostics to evaluate successful return to function. The murine system whereby mid-diaphaseal tibia fractures are imparted on the subject and fracture healing is assessed at different time points and under different therapeutic conditions is a particularly useful model to study. In this work, a novel inverse geometric nonlinear elasticity modeling framework is proposed that can reconstruct multiple mechanical properties from uniaxial testing data. To test this framework, the Lame' constants were reconstructed within the context of a murine cohort (n=6) where there were no differences in treatment post tibia fracture except that half of the mice were allowed to heal 4 days longer (10 day, and 14 day healing time point, respectively). The properties reconstructed were a shear modulus of G=511.2 ± 295.6 kPa, and 833.3± 352.3 kPa for the 10 day, and 14 day time points respectively. The second Lame' constant reconstructed at λ=1002.9 ±42.9 kPa, and 14893.7 ± 863.3 kPa for the 10 day, and 14 day time points respectively. An unpaired Student *t*-test was used to test for statistically significant differences among the groups. While the shear modulus did not meet our criteria for significance, the second Lame' constant did at a value $p<0.0001$. Traditional metrics that are commonly used within the bone fracture healing research community were not found to be statistically significant.

Keywords: fracture healing, murine, finite element, inverse problems, elasticity

1. INTRODUCTION

A critically important function of bone healing is that the healing tissue provides sufficient mechanical stabilization such that a return to functionality is possible. Because fracture healing is a phenomenon that modulates the mechanical stability of a broken bone, within the clinical context there is an important need to monitor the mechanical properties of a healing callus so that a clinician may detect and intervene in the event of a non-union. In addition, there is an equally important need to understand how to therapeutically promote better and more mechanically stable fracture healing. As a result, many researchers are studying fracture healing animal models within the context of treatment therapeutics [2-8]. While a great deal of work has been targeted at assessment of healing via imaging methods [9-16], there is real need to monitor and characterize the load-bearing mechanical properties of an experimental fracture callus system in response therapeutic intervention. To date, the level of sophistication associated with these mechanical characterizations has been somewhat simplistic. Early analysis techniques used idealized assumptions regarding geometry (e.g. beam theory) and attempted to correlate force-displacement data acquired through biomechanical testing (usually three-point bending). More recently, investigators have begun to explore novel medical imaging technologies as well as more sophisticated modeling methods [17-20]. Some studies have attempted to generate statistical models whereby microCT metrics are correlated with the results of torsional strength experiments [17, 18]. In these approaches, the challenge is that callus' often have a great deal of geometric complexity under similar initial conditions. This creates difficulty in generating proper normalized metrics such that large sample sizes are not necessary. Others have begun to explore the use of subject-specific finite element (FE) models. However these studies tend to compare empirical

torsional strength data of the specimen to simulated data whereby the objective is to determine a mathematical relationship between mechanical properties and microCT intensity [19]. The difficulty with this approach is that each system (e.g. different therapeutics, healing time point, initialization, etc.) could potentially generate a different relationship. Establishing these relationships would require many mice per system which could prove to be cumbersome.

In this paper, an approach is investigated which looks at the problem more within the context of an inverse finite element (FE) methodology. In previous work, the approach was reported using a linear Hookean elastic model of the callus [1]. It analyzed the 10-day and 14-day healing time point data reported here and found that the inverse-based metric was the only metric to show statistical significance. The unusual aspect to the work reported in this paper is that it tries to take advantage of the inherent geometric nonlinear nature of deforming soft tissue to discern more information regarding callus mechanical properties. More specifically, by incorporating an incremental moving mesh strategy, each data point along the force/displacement testing curve becomes a solution to a unique elastic problem and increases the degrees of freedom for fitting material properties. The results reported below show a considerable improvement to the statistical significance.

2. METHODS

2.1 Geometric Nonlinear Approach to an Inverse Elasticity Analysis

A linear elastic continuum is one of the fundamental models used in many biomechanics applications. To reflect this, Hooke's Law is the widely used constitutive law for representing the stress-strain behavior of the material. The model speaks to the basic principle of mechanical equilibrium and can be represented by the partial differential equation,

$$\mathbf{G}\nabla^2\bar{\mathbf{u}} + (\mathbf{G}+\lambda)\nabla(\nabla\bullet\bar{\mathbf{u}}) = 0 \qquad (1)$$

where **G** is the shear modulus, **λ** is the second Lame' constant, and $\bar{\mathbf{u}}$ is the displacement vector. With respect to usual computational practice, equation (1) would be solved using some sort of numerical technique such as the finite element method. In so doing, a geometric mesh would be generated, the partial differential equations (PDEs) would be integrated over each of the mesh subunit domains, collected into a matrix of equations, and the displacements would be solved throughout the domain simultaneously. Conventionally, this represents a linear solution, i.e. a solution to a particular boundary valued problem in this manner is unique and scalable (e.g. scaling the boundary contributing boundary conditions scales the solution by the same factor). One interpretation of a geometric nonlinear framework would be to represent the boundary conditions incrementally, and with the application of each increment, the geometric domain is altered. This results in a path dependence based on shape change for the elastic domain as well as the final solutions being presented as an accumulation of increments. Figure 1 illustrates the concept of a geometric nonlinear problem. In Figure 1a, the computation model is based on the first state of the callus. From that statement, a boundary condition set is applied that deforms the system **δ**. Upon the completion, the model from first state is executed again

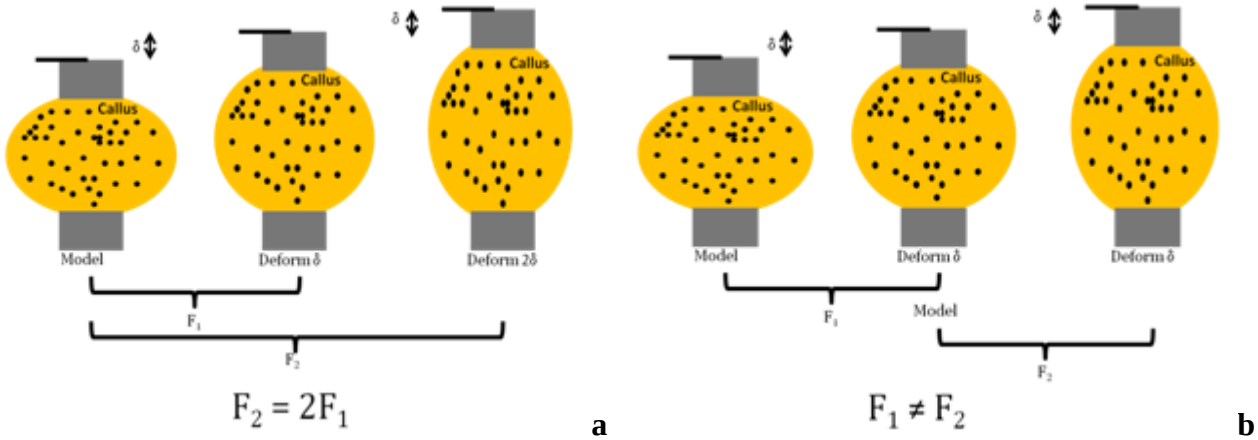

Figure 1. (a) 3 callus states whereby the model is based on state 1 and displacement **δ** is applied twice from the base state, (b) 3 callus states whereby the model is based on state 1, a displacement **δ** is applied, the model is reconstituted in its deformed state, and second displacement **δ** is applied.

with a boundary condition displacement reflecting twice that of δ. In this case, the solution to the second problem need not be constituted because it only represents a scaling of the first (just multiplying the first solution by the scale factor 2 in this is sufficient). Similarly, if one were to reconstruct the force profile that generated the displacement δ, the finding would be that twice the force is necessary for the second state. This represents the nature of a linear solution to a PDE on a fixed domain. In Figure 1b, a change can be seen. In this solution, the mesh is allowed to deform to a new shape based on the initial boundary condition application of δ. From this new domain shown in state 2, another δ boundary condition displacement is applied. In this case, if I were to constitute the forces applied between state 1 and state 2, and between state 2 and state 3, they would not be equal. This is because the shape of the domain has changed and in so doing the manner in which stress is conveyed has changed.

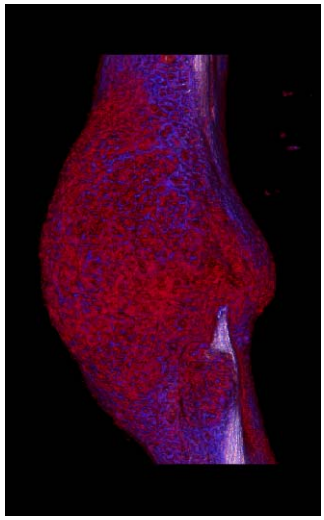

Figure 2. Image showing callus consistency. Rendering utilizes transparency to reflect bone composition with (red) cartilage, (blue) new bone, and (white) highly mineralized bone.

We hypothesize that by taking into account geometrically nonlinear effects within an inverse reconstruction framework that multiple properties can be differentiated from uniaxial testing data. More specifically, we propose to model the geometric nonlinearity in a similar manner as the above descriptive example whereby with each increment we deform the mesh and then impart the next increment. The measured forces are then determined by accumulating the differential increments. It should also be noted that for this paper the callus is being 'lumped', i.e. characterized, as one region with unique mechanical properties. Figure 2 illustrates the typical callus region extracted from μCT data and its geometrical complexity consisting of cartilage (red), new bone (blue), and highly mineralized bone (white). Observing Figure 2, one can easily note that in a dynamic mesh FE calculation, the callus constituents will change in relation to each other spatially which will ultimately translate to changes in the incremental force. While this approach is interesting, there are some inherent problems too that will also be discussed. However, in this preliminary investigation, it was intriguing to note the improvement in significance between the two mouse groups as the results will indicate.

The model equations for our system are shown in equation (1) with the caveat that a dynamic grid will be utilized in the construction process. With an initial guess at these material parameters, a finite element model of the domain shown in Figure (2) can be constructed, analogous displacements are imposed that match the experimental counterpart, and an average force (F_{calc}) is reconstructed from the simulation. A custom-built Levenberg-Marquardt non-linear optimization algorithm is then used to iteratively optimize the material properties such that the least squared error between F_{calc} and the experimental material tester generated force, F_{exptl}, is minimized. Ultimately this translates to the objective function,

$$\Psi(G,\lambda) = \sum_{i=1}^{N} \left(F_{calc} - F_{exptl}\right)_i^2 \qquad (2)$$

where N is the number of displacement data points along the elastic region of the force-displacement curve. The goal is to minimize this objective function with respect to two mechanical properties, G and λ, of the 'lumped' callus region. To optimize this for the callus properties, the derivative of our objective function, $\Psi(G,\lambda)$, is taken with respect to the properties G and λ, and set equal to zero, i.e.

$$\begin{bmatrix} \frac{d\Psi(G,\lambda)}{dG} \\ \frac{d\Psi(G,\lambda)}{d\lambda} \end{bmatrix} = \begin{bmatrix} \frac{\partial F_{calc1}}{\partial G} & \frac{\partial F_{calc2}}{\partial G} & \cdots & \frac{\partial F_{calcN}}{\partial G} \\ \frac{\partial F_{calc1}}{\partial \lambda} & \frac{\partial F_{calc2}}{\partial \lambda} & \cdots & \frac{\partial F_{calcN}}{\partial \lambda} \end{bmatrix} \begin{Bmatrix} F_{calc1} - F_{exptl1} \\ F_{calc2} - F_{exptl2} \\ \vdots \\ F_{calcN} - F_{exptlN} \end{Bmatrix} = \begin{bmatrix} 0 \\ 0 \end{bmatrix}, \qquad (3)$$

or simplified as,

$$[J]^T \left\{\overline{F}_{calc} - \overline{F}_{exptl}\right\} = 0 \qquad (4)$$

where [J] is the Jacobian matrix. It is important to note that in the above equation each component of the Jacobian is independent and is built over a series of incremental developments. In the case of a fixed mesh/grid counterpart to this approach, each subsequent strain state is just a scalar multiple based on the applied deformations. The standard Levenberg-Marquardt framework contains considerably more information and can be implemented such that multiple mechanical property reconstruction is possible, i.e.

$$\left(\left[J\right]^T\left[J\right]+\alpha I\right)\left[\Delta\overline{P}\right]=\left[J\right]^T\left\{\overline{F}_{calc}-\overline{F}_{exptl}\right\}, \quad (5)$$

and

$$\left[\Delta\overline{P}\right]=\begin{bmatrix}G\\ \lambda\end{bmatrix}_{i+1}-\begin{bmatrix}G\\ \lambda\end{bmatrix}_{i}, \quad (6)$$

with the regularization term α defined as,

$$\alpha=\left(\phi * \text{trace}\left(\left[J\right]^T\left[J\right]\right)* SSE^2\right)^{1/2} \quad (7)$$

[21], where ϕ is an empirical factor, and SSE is the sum squared error between measured and calculated force. It should be noted that the Jacobian was determined by a finite difference calculation which was initiated by a 2.5% perturbation from the initial guess of the callus property. The process is iterative until the relative error between iterations converges below a set tolerance or until no improvement in objective function is noted. With respect to reporting the values in this paper, the Lame' constants were reported but they were also converted to Young's modulus and Poisson's ratio for the purpose of comparing with the more traditional metrics and the results from [1].

2.2. Experimental Murine System

Female syngenic FVB mice (FVB-NJ, Jackson Laboratories) 8 to 12 weeks old were anesthetized using isofluorane to provide deep anesthesia. Pin stabilized mid-diaphyseal tibia fractures were generated by insertion of a 0.25 mm stainless steel pin (Fine Science Tools) through the tibial tuberosity followed by fracture creation using a three point bending device with a standardized force. Immediately following tibia fracture, 0.5 mg/kg of bupremorphine was administered for pain control. On the specified post-fracture day, mice were euthanized, fractured tibias were dissected and wrapped in phosphate buffered saline (PBS) soaked gauze and stored at -80 °C until further analysis. Using this methodology, a preliminary study (n=6) was conducted where there were no differences in treatment post tibia fracture except that half of the mice were allowed to heal 4 days longer (10 day, and 14 day healing respectively)[1]. Intuitively, mice allowed to heal longer should have a more stabilized callus (i.e. stiffer) in the fracture region. The results of that study are reported below. All animal studies were approved by the Institutional Animal Care and Use Committee at Vanderbilt University Medical Center.

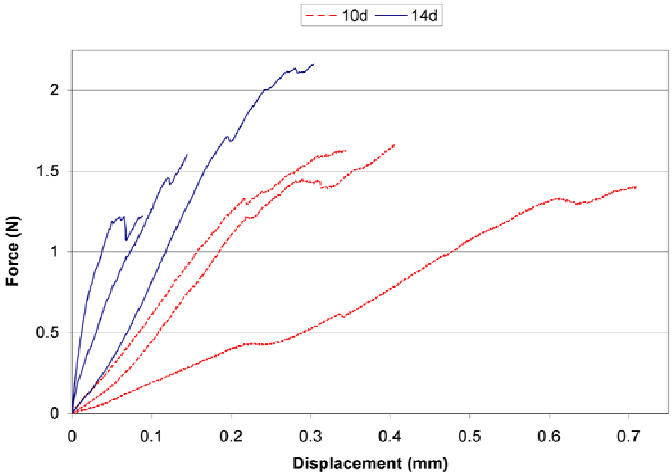

Figure 3. BMT force versus displacement data reproduced from [1] of each tibia fracture callus tested at day 10 and day 14 post fracture during distraction-to-failure testing. Note the wide sample variation within each group, demonstrating confounding geometrical effects.

CT scans of the extracted specimens were performed using a Scanco microCT 40 scanner (Scanco Medical) and were obtained at 55 kVp, 145 µA, 300 ms integration time using 12 µm voxel resolution along 5.2 mm length centered at the fracture line with a total scanning time of approximately 1 hour [18]. Figure 2 is an example of a microCT volume of data from this preliminary fracture/callus healing study[1]. These microCT reconstructions were then used for subsequent FE analysis and volume measurements.

As inverse techniques require true data comparison to effectively reconstruct callus elastic properties, fractured tibia ends were embedded into a polymethylmethacrylate cast using custom designed testing fixtures, leaving the fracture callus exposed. Specimens are kept fully hydrated with PBS during the entire testing procedure. The fixtures were loaded into the mechanical tester (Enduratec ELF 3100) and tested in tension at a fixed displacement rate of 0.25 mm/min using a 22 N transducer (Honeywell Sensotec) [22]. Displacement and force data were recorded until failure. Reproduced from [1], Figure 3 shows the data from all 6 subjects. While distinction among the two groups can be seen visually, there is a significant amount of spread within each group.

3. RESULTS

	10 d (n=3)	14 d (n=3)	P Value
Ultimate Load (N)	1.56 ± 0.14	1.64 ± 0.49	0.79
Toughness (N*mm)	0.41 ± 0.088	0.20 ± 0.16	0.11
Apparent Stiffness (N/mm)	4.74 ± 2.35	14.0 ± 6.2	0.08
Normalized Apparent Stiffness (kPa)	3885.3 ± 1799.7	8330.1 ± 4941.0	0.22
$G_{linear\ recon}$ (kPa)	274.9 ± 142.9	1002.9 ± 301.0	0.019*
$G_{non\text{-}linear\ recon}$ (kPa)	511.2 ± 295.6	833.3 ± 352.3	0.29
$\lambda_{non\text{-}linear\ recon}$ (kPa)	1002.9 ± 42.9	14893.7 ± 863.3	<0.0001*

Table 1. Results for biomechanical testing (BMT) metrics for 10day and 14day mice.

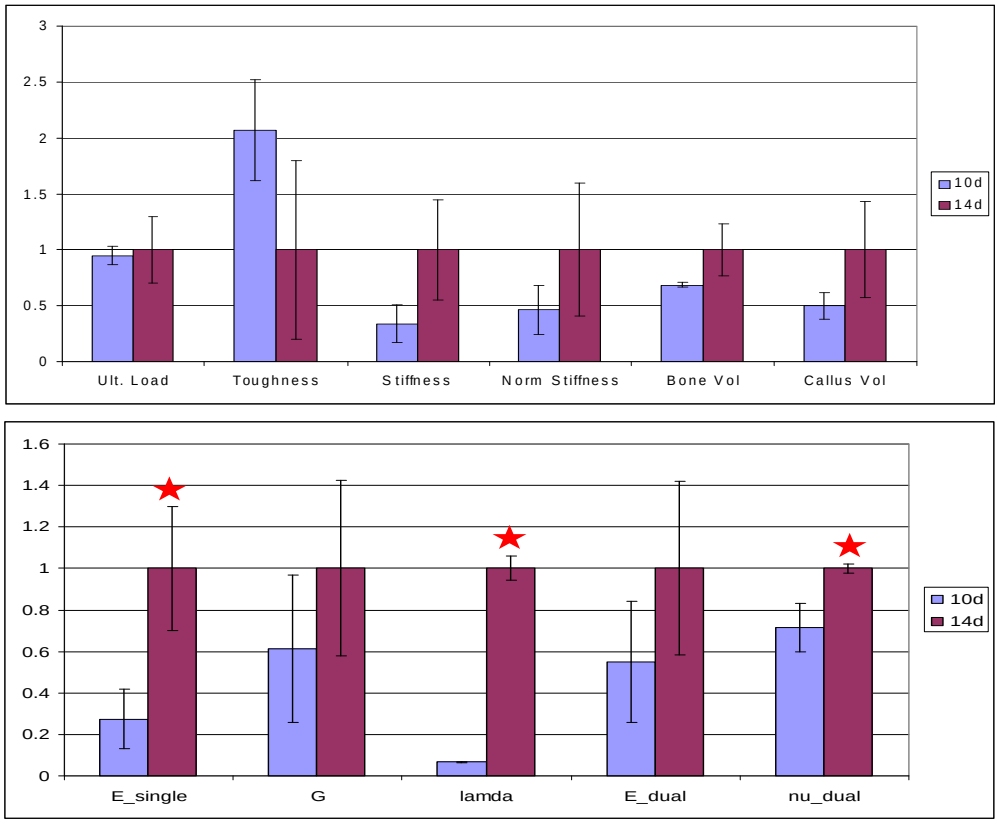

Figure 4. (a) Routine BMT metrics for each mice group, (b) reconstruction properties with the single property reconstruction, reconstructed Lame' constants, followed transformed Lame' constants into Young's modulus and Poisson's ratio (red star indicates statistical significance with $p < 0.05$). Each has been normalized by the 14 day value.

Table 1 illustrates the results of the reconstruction as well as the comparison of the linear reconstruction from [1]. Figure 4a illustrates the mean and standard deviation of routine biomechanical testing metrics while Figure 4b illustrates the

reconstructed material parameters with the linear reconstructed Young's modulus, followed by the nonlinear reconstructed Lame' constants, and the reformatted nonlinear values into Young's modulus and Poisson's ratio (note each has been normalized by its 14-day value).

4. DISCUSSION

Table 1 and Figure 4 are encouraging in that the nonlinear reconstruction differentiated the two groups more significantly than its linear counterpart (it should be noted that the linear reconstruction used a constant Poisson's ratio, ν=0.45). The other intriguing aspect is that the Lame' constant λ was found to be statistically different between groups while the shear modules did not reflect this level of difference. It is likely that given the heterogeneous nature of a healing callus, volumetric changes probably dominate its load/displacement behavior as opposed to constant-volume distortional shape change.

While the results are suggestive, the methods reported have shortcomings at this early stage. Some of those short comings are: (1) lack of finer discretization of the callus models, (2) the choice of tetrahedral elements as opposed to ones more accurate in mechanics modeling, e.g. hexahedral elements [23], (3) although the grid is dynamic in the geometric nonlinear approach, the lack of re-meshing for the intermediate steps to ensure optimal element aspect ratios, (4) the high strain conditions within the fracture fissure likely need the full-nonlinear strain tensor description, (5) lack of more data necessary to achieve statistical significance, (6) the inherent experimental error associated with 'potting' tibia fractures and mechanical testing, and (7) determining how much measurement change occurs as a result of nonlinear shape change during mechanical excitation and whether the sensitivity of the force transducer can detect that change.

5. CONCLUSIONS

A method to reconstruct multiple material properties from uniaxial BMT data using geometrically nonlinear information is presented. An initial study using 6 mice separated into 2 groups differing by an extra 4 days of healing was used as a system to test the inverse elastic property reconstruction. Using the enhanced method, better statistical difference between the groups was achieved. In future work, shortcomings will be addressed as well as future testing of the frameworks within the context of therapeutic challenges.

6. ACKNOWLEDGEMENTS

This work was supported by National Institutes of Health (NIH) Grant 5R01DK070929-02 from the National Institute of Diabetes and Digestive and Kidney Diseases (NIDDK).

7. REFERENCES

[1] J. A. Weis, M. I. Miga, F. Granero-Molto, and A. Spagnoli, "A finite element inverse analysis to assess functional improvement during the fracture healing process," *Journal of Biomechanics,* 2009 (in press).

[2] F. Granero-Molto, J. A. Weis, L. Longobardi, and A. Spagnoli, "Role of mesenchymal stem cells in regenerative medicine: application to bone and cartilage repair," *Expert Opinion on Biological Therapy,* vol. 8, pp. 255-268, 2008.

[3] F. Granero-Molto, J. A. Weis, L. D. O'Rear, M. I. Miga, and A. Spagnoli, "IGF-I engineered bone marrow mesenchymal stem cells improve the fracture healing process," *Journal of Bone and Mineral Research,* vol. 22, pp. S105-S105, 2007.

[4] G. E. Gutierrez, J. R. Edwards, I. R. Jarrett, J. S. Nyman, B. Mccluskey, G. Rossini, A. Flores, D. B. Neidre, and G. R. Mundy, "Transdermal Lovastatin Enhances Fracture Repair in Rats," *Journal of Bone and Mineral Research,* vol. 23, pp. 1722-1730, Nov 2008.

[5] G. Holzer, R. J. Majeska, M. W. Lundy, J. R. Hartke, and T. A. Einhorn, "Parathyroid hormone enhances fracture healing - A preliminary report," *Clinical Orthopaedics and Related Research,* pp. 258-263, Sep 1999.

[6] P. M. Huddleston, J. M. Steckelberg, A. D. Hanssen, M. S. Rouse, M. E. Bolander, and R. Patel, "Ciprofloxacin Inhibition of Experimental Fracture-Healing," *The Journal of Bone & Joint Surgery,* vol. 82, pp. 161-173, 2000.

[7] T. Zachos, A. Diggs, S. Weisbrode, J. Bartlett, and A. Bertone, "Mesenchymal stem cell-mediated gene delivery of bone morphogenetic protein-2 in an articular fracture model," *Molecular Therapy,* vol. 15, pp. 1543-1550, Aug 2007.

[8] M. Zhao, Z. Zhao, J. T. Koh, T. C. Jin, and R. T. Franceschi, "Combinatorial gene therapy for bone regeneration: Cooperative interactions between adenovirus vectors expressing bone morphogenetic proteins 2, 4, and 7," *Journal of Cellular Biochemistry,* vol. 95, pp. 1-16, May 1 2005.
[9] W. K. Hsu, B. T. Feeley, L. Krenek, D. B. Stout, A. F. Chatziioannou, and J. R. Lieberman, "The use of F-18-fluoride and F-18-FDG PET scans to assess fracture healing in a rat femur model," *European Journal of Nuclear Medicine and Molecular Imaging,* vol. 34, pp. 1291-1301, Aug 2007.
[10] R. Schmidhammer, S. Zandieh, R. Mittermayr, L. E. Pelinka, M. Leixnering, R. Hopf, A. Kroepfl, and H. Redl, "Assessment of bone union/nonunion in an experimental model using microcomputed technology," *Journal of Trauma-Injury Infection and Critical Care,* vol. 61, pp. 199-205, 2006.
[11] S. Ciprian, S. Iochum, R. Kohlmann, G. Dautel, F. Dap, and A. Blum, "MR imaging accuracy in the prediction of bone graft healing potential in scaphoid non-union," *Journal De Radiologie,* vol. 85, pp. 1699-1706, 2004.
[12] J. A. Lynch, M. Grigoryan, A. Fierlinger, A. Guermazi, S. Zaim, D. B. MacLean, and H. K. Genant, "Measurement of changes in trabecular bone at fracture sites using X-ray CT and automated image registration and processing," *Journal of Orthopaedic Research,* vol. 22, pp. 362-367, 2004.
[13] A. E. Severns, Y. P. Lee, S. D. Nelson, E. E. Johnson, and J. M. Kabo, "Metabolic measurement techniques to assess bone fracture healing - A preliminary study," *Clinical Orthopaedics and Related Research,* pp. 231-238, 2004.
[14] M. Grigoryan, J. A. Lynch, A. L. Fierlinger, A. Guermazi, B. Fan, D. B. MacLean, A. MacLean, and H. K. Genant, "Quantitative and qualitative assessment of closed fracture healing using computed tomography and conventional radiography," *Academic Radiology,* vol. 10, pp. 1267-1273, 2003.
[15] H. C. Cattermole, J. N. Fordham, D. S. Muckle, and J. L. Cunningham, "Dual-energy x-ray absorptiometry as a measure of healing in fractures treated by intramedullary nailing," *Journal of Orthopaedic Trauma,* vol. 10, pp. 563-568, 1996.
[16] N. Saran and R. C. Hamdy, "DEXA as a Predictor of Fixator Removal in Distraction Osteogenesis," *Clinical Orthopaedics and Related Research,* vol. 466, pp. 2955-2961, 2008.
[17] E. F. Morgan, Z. D. Mason, K. B. Chien, A. J. Pfeiffer, G. L. Barnes, T. A. Einhorn, and L. C. Gerstenfeld, "Micro-computed tomography assessment of fracture healing: Relationships among callus structure, composition, and mechanical function," *Bone,* vol. 44, pp. 335-344, Feb 2009.
[18] D. G. Reynolds, C. Hock, S. Shaikh, J. Jacobson, X. P. Zhang, P. T. Rubery, C. A. Beck, R. J. O'Keefe, A. L. Lerner, E. M. Schwarz, and H. A. Awad, "Micro-computed tomography prediction of biomechanical strength in murine structural bone grafts," *Journal of Biomechanics,* vol. 40, pp. 3178-3186, 2007.
[19] S. J. Shefelbine, U. Simon, L. Claes, A. Gold, Y. Gabet, I. Bab, R. Muller, and P. Augat, "Prediction of fracture callus mechanical properties using micro-CT images and voxel-based finite element analysis," *Bone,* vol. 36, pp. 480-488, Mar 2005.
[20] J. A. Weis, F. Granero-Molto, L. D. O'Rear, M. I. Miga, and A. Spagnoli, "Development of a high-resolution 3D Micro-CT based model to predict fracture callus histological architecture," *Journal of Bone and Mineral Research,* vol. 22, p. W472, 2007.
[21] N. Joachimowicz, C. Pichot, and J. P. Hugonin, "Inverse Scattering - an Iterative Numerical-Method for Electromagnetic Imaging," *IEEE Transactions on Antennas and Propagation,* vol. 39, pp. 1742-1752, Dec 1991.
[22] C. Colnot, Z. Thompson, T. Miclau, Z. Werb, and J. A. Helms, "Altered fracture repair in the absence of MMP9," *Development,* vol. 130, pp. 4123-4133, Sep 2003.
[23] S. E. Benzley, E. Perry, K. Merkley, B. Clark, and G. Sjaardema, "A Comparison of All-Hexahedral and All-Tetrahedral Finite Element Meshes for Elastic and Elasto-Plastic Analysis," in *Proc. 4th International Meshing Roundtable*, Sandia National Laboratories, 1995, pp. 179-191.